Int. J. Electrochem. Sci., 17 **(2022)** Article Number: 220211, doi: 10.20964/2022.02.17

International Journal of
ELECTROCHEMICAL
SCIENCE
www.electrochemsci.org

Development of Electrochemiluminescence Immunosensor based Sandwich Structure Composites for Determination of Serum Insulin Level in Athletes

Naihong Liu[1], *Dandan Cao*[1], *Ye Wu*[2,*], *Youjun Wang*[3,*]

[1] College of Physical Education, Taiyuan University of Science and Technology, Taiyuan, 030024, China
[2] School of Basic Medical Sciences, Capital Medical University, Beijing, 100069, China
[3] Department of Taichi and Martial Arts, Jiaozuo University, Jiaozuo, 454002, China
[*]E-mails: nh_liu@126.com, wyj9120902@163.com

Received: 8 October 2021 / *Accepted:* 24 November 2021 / *Published:* 5 January 2022

The goal of this work was to develop an electrochemiluminescence (ECL) immunosensor based on the luminol-O_2 technology for measuring serum insulin levels in athletes. For construction of the sandwich-configuration electrochemiluminescence immunoassay, the Au and CeO_2 nanocomposite electrodeposited on functionalized CNTs (Au@CeO_2/f-CNTs) and combined with luminol (Lu/Au@CeO_2/f-CNTs), and the nanocomposite of dopamine@SiO_2 (DA@SiO_2) used as quencher of ECL signal. The primary antibody (Ab_1) and secondary antibody (Ab_2) modified the composite surface of DA@SiO_2 and Au@CeO_2/f-CNTs, respectively for enhancement of sensitivity of immunosensor. SEM and XRD analyses confirmed successful synthesis of DA@SiO_2 and Au@CeO_2/f-CNTs nanocomposites. The optimal condition were investigated for achievement of maximum ECL signal, and results showed under the optimal experimental conditions, immunosensor showed high sensitivity and anti-interference capability to determination of insulin, and the detection limit and linear range of immunosensor were obtained 17 ng/ml and 10-4 ng/ml to 50 ng/ml, respectively. The precision and applicability of the proposed ECL immunosensor to determination of insulin were investigated in blood serum specimens of athletes as real samples, and results indicated to the acceptable recovery (100.60 to 94.85%) and RSD (3.11 to 1.84 %) values, and verification of feasibility of the proposed ECL immunosensor for determination of serum insulin level in athletes.

Keywords: Insulin; Electrochemiluminescence immunosensor; Au nanoparticles; CeO_2 nanoparticles; functionalized CNTs; dopamine@SiO_2 nanocomposite

1. INTRODUCTION

Insulin ($C_{257}H_{383}N_{65}O_{77}S_6$) is a hormone made in the pancreas that helps the human body to use glucose for energy. Insulin helps keep the blood sugar level from getting too high [1, 2]. Human

insulin consists of two peptide chains named as A-chain and B-chain that the peptide chains are linked together by two disulfide bonds, and A-chain and B-chain are composed of 21 and 30 amino acids, respectively [3, 4]. Moreover, diabetes mellitus is a chronic disease and potentially life-threatening condition that occurs either when the pancreas does not produce enough insulin or when the body cannot effectively use the insulin it produces, resulting in blood glucose levels that are too high [5]. Hyperglycaemia, or raised blood sugar is a common effect of uncontrolled diabetes and over time leads to serious damage to many of the body's systems, especially the nerves and blood vessels [6, 7].

Furthermore, the maintaining insulin infusion sets during exercise and sport has been an important challenge [8-10]. After exercise, insulin-independent glucose uptake by muscles remains elevated for approximately two hours. Insulin sensitivity also enhances after exercise [11]. By taking insulin and glucose simultaneously, while steroids spawn new muscle, insulin boosts glycogen production, insulin inhibits catabolism in muscle and liver by increasing the synthesis of glycogen and proteins and promoting the entry of glycogen and amino acids into muscle cells before an event, thereby improving stamina [12, 13]. An athlete's stamina is determined by his or her ability to store glycogen. Insulin is also a commonly used as performance enhancing drug by body builders for its purported anabolic properties such as stimulation of glycogen formation, which is important for muscle recovery after exercise [14-16]. Accordingly, insulin was banned by the International Olympic Committee in 1998. Athletes with insulin-requiring diabetes may use insulin with a medical exemption [17].

Therefore, determination the insulin level in biological fluids of athletes and patients has been the important issue and many studies have been conducted to optimize and enhance the precision of assay techniques which contained high-performance liquid chromatography, fluorescence, ultraviolet and luminescence detection, electrophoresis, mass spectrometry, electrochemical biosensor and immunoassays [18-20]. Among them, the electrochemiluminescence immunoassay shows the high sensitivity and selectivity due to modification capability of the detection systems in sandwich structures with antibodies and nanomaterials which can amplify signals to enhance light levels [21]. Therefore, this study was performed to construct a novel electrochemiluminescence immunosensor based on sandwich structure of Au@CeO_2/f-CNTs and Ab_2/DA@SiO_2 and application in the measurement of serum insulin level in athletes.

2. MATERIALS AND METHOD

2.1 Preparation of Ab_1/Lu/Au@CeO_2/f-CNTs and Ab_2/DA@SiO_2

Electrochemical deposition technique was applied for modification of the GCE with f-CNTs and Au@CeO_2/f-CNTs [22-24]. Prior the modification, the bare GCE was polished to a mirror-like surface with alumina slurry (≥99%, 1.0, 0.3, and 0.05 μm, Merck, Germany) on a polishing pad for 15 minutes, and then ultrasonically washed in mixture of deionized water and ethanol (95%, Shandong Aojin Chemical Technology Co., Ltd., China) in equal volume ratio for 5 minutes. In order

to create the supportive growth centers on the GCE surface, the clean GCE was functionalized through the immersion in 1M nitric acid (65%, Merck, Germany) under magnetic stirring at 75°C for 6 hours [25]. After then, the GCE was rinsed with deionized water and dried at room temperature. The CNTs (≥90%, Easy material Group Limited, China) were functionalized in a chemical solution of sulphuric acid (97%, Merck, Germany) and nitric acid with volume ratio of 3:1 at 60 °C for 5 hours. Next, f-CNTs were separated by filtration, washed with deionized water, and transferred into an oven at 75°C for 5 hours to complete drying [26]. The electrochemical deposition of f-CNTs on GCE was conducted on potentiostat/galvanostat electrochemical workstation (CS350/CS16X, Xian Yima Optoelec Co., Ltd., China) in electrochemical cell, containing GCE as working electrode, platinum wire as counter electrode, and Ag/AgCl (3M KCl) as reference electrode. The electrodeposition was carried out in 1.0 g/l f-CNTs in 0.1M phosphate buffer solution (PBS) pH 7.4 at potential range of -1.3 V to +0.7 V at scan rate of 10 mV/s for 15 minutes. 0.1M PBS were prepared using a mixture of Na_2HPO_4 (99%, Merck, Germany).and NaH_2PO_4 (99%, Merck, Germany). Electrodeposition of Au@CeO_2 NPs on GCE or f-CNTs/GCE was performed at potential range of -1.3 V to -0.5 for 15 minutes in the electrolyte solution was prepared from mixture of 20ml of A 0.1 M $Ce(NO_3)_3$ (99.9%, Sigma-Aldrich) and 20ml of $KAu(CN)_2$ (≥99%, Sigma-Aldrich) aqueous solutions. Au-CeO_2/f-CNTs/GCE was immersed in 2 mL of 1 mM luminol (Lu, 97%, Sigma-Aldrich) solution for 24 hours. Afterward, the electrode was rinsed with deionized water. Subsequently, the Lu/Au@CeO_2/f-CNTs/GCE was immersed in Ab_1 (insulin antibody, Sigma-Aldrich) for 15 minutes, then rinsed with deionized water to remove unattached Ab_1. Finally, Ab_1/Lu/Au@CeO_2/f-CNTs/GCE was immersed 0.1M PBS pH 7.4 and stored at 4°C stored in the refrigerator at 4°C for future use.

For synthesis the SiO_2, the first mixture of 12 mM tetraethylorthosilicate (TEOS, ≥99.0%, Sigma-Aldrich), n-amyl alcohol (≥99%, Merck, Germany) and cyclohexane (≥99%, Merck, Germany) in volume ratio of 2:1:10 were stirred for 10 minutes at 35°C [27]. Then, the separated mixture was prepared from 6mM cetyltrimethylammonium bromide (CTAB, ≥98%, Sigma-Aldrich), urea (99%, Sigma-Aldrich) and deionized water in volume ratio of 2:1:10. After that, the first mixture was added to the second mixture and stirred for 30 minutes at room temperature. The obtained mixture was loaded into a Teflon-lined stainless-100 ml steel autoclave, sealed, and maintained at 115°C for 5 hours. After cooling, the resulting product was washed with acetone (99%, Shandong Bilifu Chemical Co., Ltd., China) and deionized water, respectively, and dried in the oven at 500°C or 5 hours. For preparation of dopamine@SiO_2 composite, 0.1 g dopamine (DA, 98%, Sigma-Aldrich) was ultrasonically dissolved in 20 mL of 12 mM Tris hydrochloride (99%, Sigma-Aldrich) solution. Next, the obtained solution was mixed with the 0.1 g SiO_2 under magnetic stirring for 12 hours at room temperature. Thereupon, the obtained product was centrifuged at 1500 rpm for 10 minutes and dried at room temperature. Furthermore, 4 mg of obtained powder was dissolved into 2 mL of 0.1M PBS pH 7.4. To synthesize Ab_2/DA@SiO_2, 300 µL of Ab_2 was added to the 2 mL of DA@SiO_2 mixture under magnetic stirring, then rinsed with deionized water to remove unattached Ab_2, and dispersed in 4mL of 0.1M PBS pH 7.4 and stored at 4°C stored in refrigerator at 4°C.

2.2 Preparation of the sandwich ECL immunosensor

In order to fabrication the ECL immunosensor, Ab_1/Lu/Au@CeO_2/f-CNTs/GCE was covered with 5µL of bovine serum albumin (BSA, 1%, Sigma-Aldrich) for blocking the possible remaining active sites avoiding any nonspecific adsorption at 4 °C [28]. Then, the electrode was rinsed with 0.1M PBS pH 7.4, and 5 µL of insulin antigen (IAg, Sigma-Aldrich) was dropped onto the modified electrode surface, followed by washing with 0.1M PBS and drying with nitrogen. Eventually, 5 µL of 5g/l Ab_2/DA@SiO_2 was incubated on electrode surfaces overnight at *4*°C and dried with nitrogen. The obtained modified immunosensor was rinsed with 0.1M PBS and stored at 4 °C for later use.

2.3 Characterization

The ECL studies was performed in 0.1mM carbonate buffered saline (CBS) solution pH 7.5 which prepared from 0.1 mM Na_2CO_3 (≥95%, Sigma-Aldrich) and 0.1 mM $NaHCO_3$ (≥99%, Sigma-Aldrich) in equal ratio. Electrochemical impedance spectroscopy (EIS) analyses of bare GCE and modified GCE were carried out using potentiostat/galvanostat electrochemical workstation in three-electrode electrochemical cell in 5 mM $[Fe(CN)_6]^{3-/4-}$ (≥99%, Sigma-Aldrich) solution containing 0.1 M KCl (≥99%, Merck, Germany) as the supporting electrolyte within the frequency range of 10mHz to 10^2 kHz at biasing potential of 10 mV. The ECL measurements were conducted on MPI-F flow-injection chemiluminescence detector (Xi'an remax Electronic Science Tech. Co. Ltd., China), and the voltage of the photomultiplier tube (PMT) was set at 500 V. The measurements were carried out using the single-cycle pulse that included the 0.5 V as pulse potential, 0.1 s pulse time, -0.5 V as initial potential, and 10 s pulse period. In order to study the selectivity and anti-interference capability of the prepared immunosensor all of interfernant agents were provided from Sigma-Aldrich. The morphological and structural analyses of prepared samples were carried out using scanning electron microscopy (SEM, SU-8010, Hitachi, Japan) and X-ray diffractometer (XRD, D8-FOCUS, Bruker AXS GmbH, Germany), respectively. The enzyme-linked immunosorbent assay kit (ELISA, LS-F21892, optical density at 450 nm, LifeSpan Bioscience, Inc., USA) was used for study of insulin content in human blood serum that the concentration range of its calibration plot was in the range of 0.31 - 20 ng/ml.

3. RESULTS AND DISCUSSION

3.1. Morphological and structural characterization of nanostructures

The morphological analyses of the prepared nanostructures were performed via SEM. Figure 1a shows the SEM image of surface of electrodeposited f-CNTs of GCE surface which depict a highly porous interconnected network of entangled CNT bundles. The diameter of nanotubes is 90nm. Figure 1b exhibits the SEM image of electrodeposited Au@CeO_2/f-CNTs on GCE which indicated the nanocomposite of Au@CeO_2 covered the f-CNTs surface. The nanocomposite is composed of nanoparticles in spherical shape that the average size of nanoparticles is 50nm. Large number of

Au@CeO_2 nanoparticles was embedded on the f-CNTs surface. As observed from Figure 1c, the SEM image of SiO_2 shows the mesoporous nanospheres of synthesized SiO_2 which display the porous and irregular craters structure. The average size of SiO_2 nanospheres is 145nm. The SEM image of DA@SiO_2 in Figure 1d depicts that the average size of DA@SiO_2 particles is 150nm which indicates to successful deposition of DA film was successfully deposited on the surface of SiO_2 mesoporous nanospheres.

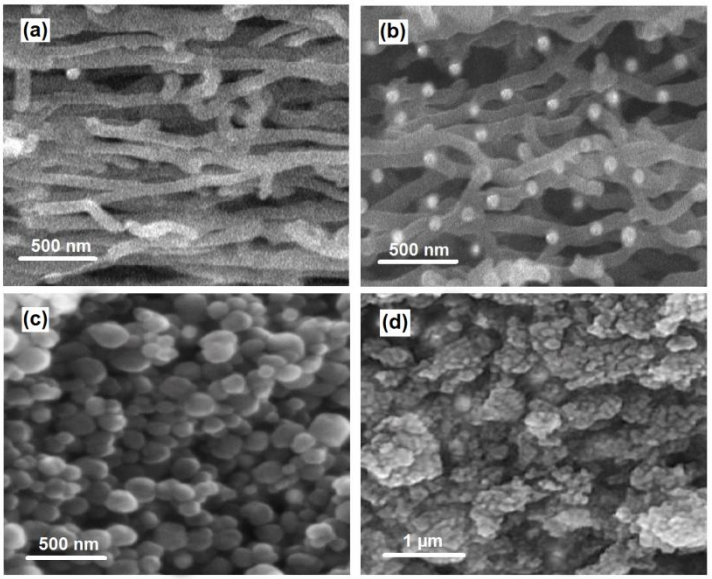

Figure 1. The SEM images of (a) electrodeposited f-CNTs and (b) Au@CeO_2/f-CNTs on GCE, and (c) synthesized SiO_2 and (d) DA@SiO_2.

Figure 2 shows the XRD patterns of powders of electrodeposited f-CNTs, CeO_2/f-CNTs and Au@CeO_2/f-CNTs on GCE surface and synthesized SiO_2 and DA@SiO_2. As observed in the XRD pattern of f-CNTs (Figure 2a), there are two diffraction peaks at 26.02° and 43.22° which indexed to (002) and (100) reflection of graphitic structure of CNTs (JCPDS card No. 96-101-1061). The XRD patterns electrodeposited CeO_2/f-CNTs in Figure 2b shows the new diffraction peaks are observed at 28.90°, 32.21°and 47.95° which can be attributed to (111), (200), (220) planes of CeO_2 in cubic fluorite-structure (JCPDS card No. 01-073-6318). The XRD patterns electrodeposited Au@CeO_2/f-CNTs in Figure 2c indicates when Au nanoparticles was introduced in the composite, the additional peaks at 38.15° and 44.29° are appeared, corresponding to formation the (111) and (200) planes of Au in cubic structure (JCPDS card No 03-065-2870), and confirms the simultaneous electrodeposition of Au and CeO_2 on f-CNTs surface. The XRD pattern of SiO_2 in Figure 2c indicates the wide band diffraction peak at 22.44°, and absence of other sharp peaks indicates the amorphous nature of the synthesized SiO_2 nanospheres [29]. The XRD pattern of DA@SiO_2 in Figure 2d shows the broad XRD reflection peak at 22.88° that the shift peak could be associated with the diffraction of the synthesized dopamine amorphous structures on SiO_2 nanospheres [30]. The XRD results are in agreement with the SEM analyses.

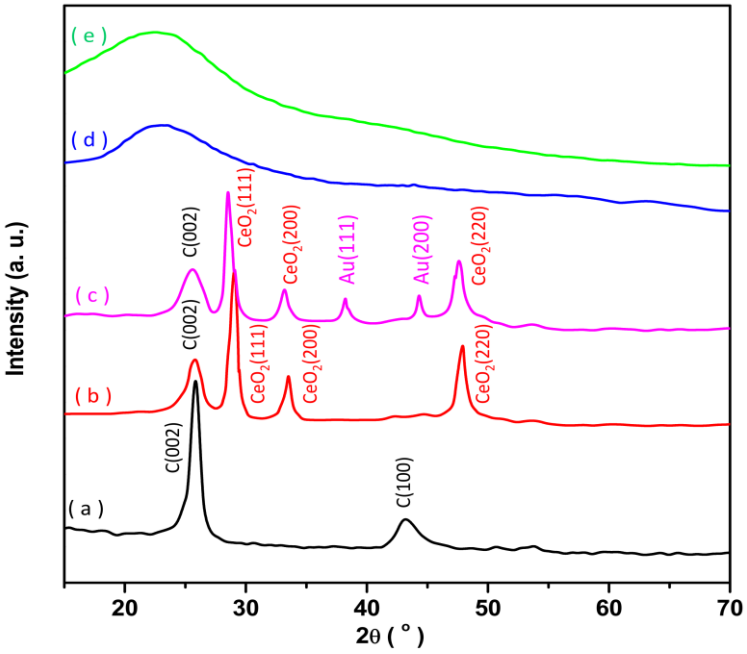

Figure 2. XRD patterns of powders of electrodeposited (a) f-CNTs, (b) CeO_2/f-CNTs and (c) Au@CeO_2/f-CNTs on GCE surface, and synthesized (d) SiO_2 and (e) DA@SiO_2.

3.2 Study of ECL immunosensor

The ECL immunosensor study in this work is based on the luminol-O_2 system which demonstrated to oxidation of luminol to LH^-, reduction of O_2 to superoxide anion radicals ($O_2^{\bullet-}$) and oxidation LH^- to LH as following equation [31]:

Luminol → LH^- (1)

$LH^- + O_2 \rightarrow LH + O_2^{\bullet-}$ (2)

As consequence, the interaction LH^- with the obtained reactive intermediates $O_2^{\bullet-}$ generates [LO_2^{2-}] that decomposes and releases nitrogen gas and forms the excited-state species 3-aminophthalate (AP*) which exists in an excited state as equations (3) and (4), respectively [31, 32].

LH- + O2 $^{\bullet-}$ → [LO_2^{2-}] (3)

[LO_2^{2-}]→ AP* +N_2 (4)

AP* relaxes to the ground state (AP) as equation (5), and produces a photon of visible light which can be observed as a chemiluminescence signal.

AP* → AP + hv (5)

Studies were mentioned that Au nanostructures can catalyze the reaction of O_2 to form $O_2^{\bullet-}$ and enhance the ECL intensity in luminol-O_2 system [33, 34]. Figure 3 shows ECL intensity of pure luminol, Lu/CeO_2/f-CNTs and Lu/Au@CeO_2/f-CNTs, illustrating Au and CeO_2 nanostructures can improve the ECL intensity of luminol. CeO_2 nanoparticles displays prominent electro-catalytic property and oxygen storage capability in electrocatalysis and has favorable amplification effect on ECL signal in luminol-dissolved O_2 system due to feasible conversion between the oxidation states of Ce^{3+} and Ce^{4+}, which can improve the formation of $O_2^{\bullet-}$ in luminol-dissolved O_2 system [35]. It can be

resulted the higher generation of AP* species for amplifying ECL intensity. Moreover, superoxo species can be formed and bonded on Au nanoparticles surface specially to positive Au atoms forming Au–O–O that the species act as the real catalytic species which cause to attack luminol to form 3-aminophthalate in its singlet excited state that relaxes to the corresponding ground state by emitting one photon [36]. f-CNTs act as the functional supporting matrix to improve the catalytic activity of Au and CeO_2 nanoparticles due high conductivity and large active surface [37]. The simultaneous electrodeposition of Au and CeO_2 on f-CNTs surface provides the synergistic enhancement effects for superior ECL performance [38].

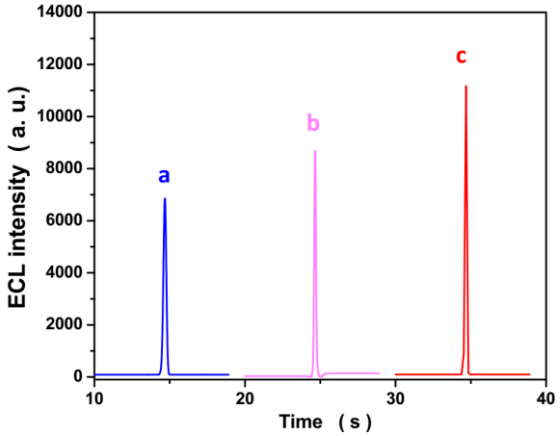

Figure 3. ECL intensity of (a) pure luminol, (b) Lu/CeO_2/f-CNTs and (c) Lu/Au@CeO_2/f-CNTs

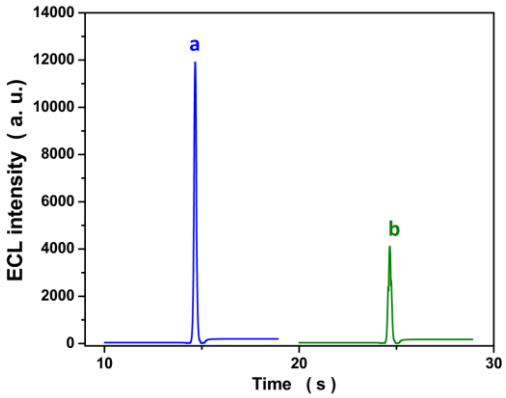

Figure 4. ECL intensity of Lu/Au@CeO_2/f-CNTs in (a) absence and (b) presence of 10000u/mg superoxide dismutase in detection solution

Figure 4a shows the ECL intensity of Lu/Au@CeO_2/f-CNTs in absence and presence of 10000u/mg superoxide dismutase in the detection solution. superoxide dismutase is well-known as a scavenger of endogenous free radicals of $O_2^{\bullet-}$ [39]. As seen, the ECL intensity of Lu/Au@CeO_2/f-CNTs is significantly quenched because of specificity of superoxide dismutase to $O_2^{\bullet-}$. The fluorescence analyses were used for investigation of the possible quenching mechanism of ECL. Figure 4b shows the fluorescence spectra of pure luminol and Lu/DA@SiO_2. It is obviously observed

that the peak of fluorescence spectra of Lu/DA@SiO_2 shows a considerable decrease compared to pure luminol which attributed to functionalities such as amines, thiols, imine and catechol groups can expose on the DA surface, and quinone units contained by DA@SiO_2 might effectively quench ECL signal intensity [40, 41].

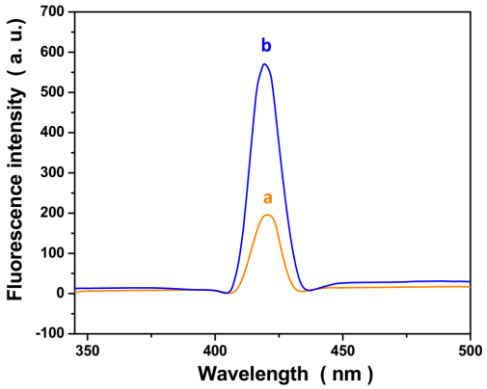

Figure 5. Fluorescence spectra of (a) pure luminol and (b) Lu/DA@SiO_2

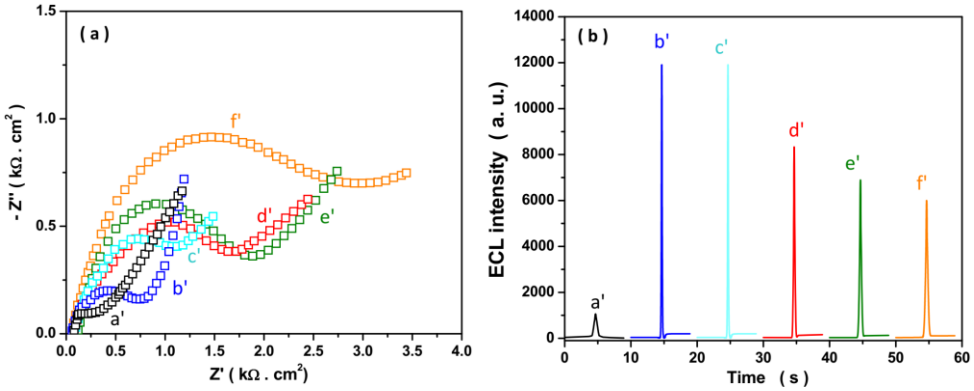

Figure 6. EIS (a) and ECL intensity (b) of (a') bare GCE, (b') Lu/Au@CeO_2/f-CNTs/GCE, (c') Ab_1/Lu/Au@CeO_2/f-CNTs/GCE, (d') BSA/Ab_1/Lu/Au@CeO_2/f-CNTs/GCE, (e') IAg/BSA/Ab_1/Lu/Au@CeO_2/f-CNTs/GCE and (f') Ab_2/DA@SiO_2/IAg/BSA/Ab_1/Lu/Au@CeO_2/f-CNTs/GCE.

In order to study the interface properties of the immunosensor, Figure 6a shows the Nyquist plots of EIS analyses of bare GCE and modified GCE in 5 mM [Fe(CN) 6] $^{3-/4-}$ solution containing 0.1 M KCl as the supporting electrolyte within the frequency range of 10mHz to 10^2 kHz a*t* biasing potential of *10* mV. As observed, there are Nyquist plots with semicircles in the high frequency area, and the linear part in the low that the diameter of the semicircle is interpreted as charge transfer resistance and linear part corresponding to diffusion resistance of the electrolyte [42, 43]. As seen, the diameter of the semicircles of bare GCE is very small which is associated with the fast electron transfer on bare GCE surface. The diameter of the semicircles of Lu/Au@CeO_2/f-CNTs/GCE is slightly increased which can be related to modification of the electrode surface using the

semiconductors. The diameter of the semicircles of Nyquist plots of Ab_1/Lu/Au@CeO_2/f-CNTs/GCE, and Ab_1/Lu/Au@CeO_2/f-CNTs/GCE after modification with BSA, IAg and Ab_2/DA@SiO_2 are gradually increased which indicted to increase the charge transfer resistance because of the nonconductive characteristics of the proteins [44].

Figure 6b shows the ECL characterization of modification steps of immunosensor. It can be observed that there is a low ECL intensity for bare GCE. After modification the GCE surface with Lu/Au@CeO_2/f-CNTs, the ECL intensity is improved remarkably that it can related to promotion of electro-catalytic property and signal-amplification effect on ECL through Au and CeO_2 nanoparticles [35-38]. Ab_1/Lu/Au@CeO_2/f-CNTs/GCE shows that the ECL intensity is decreased that related to nonconductive characteristics of the proteins, and proteins could interrupt the interfacial electron transfer and hinder the diffusion of the ECL active substances [45]. The ECL intensity continued to decrease when BSA, IAg and Ab_2/DA@SiO_2 modified the Ab_1/Lu/Au@CeO_2/f-CNTs/GCE, respectively. It can be due to non-electroactive properties of BSA, IAg and Ab_2 molecules, and can increase the steric hindrance and hinder the electron transfer [46]. Moreover, DA@SiO_2 quenches the ECL intensity of Au@CeO_2. The results illustrate that the ECL immunosensor was successfully fabricated.

In order to optimize the measurement condition, the ECL immunosensor performance as an insulin sensor was investigated in different pH values and different concentrations of Lu/Au@CeO_2/f-CNTs which play an important role in the ECL reaction process. Figure 7a shows the pH effect on the ECL response of the resulting sandwich immunosensor (Ab_2/DA@SiO_2/IAg/BSA/Ab_1/Lu/Au@CeO_2/f-CNTs). As seen, the response of ECL intensity is increased with increasing the pH value up to 7.5, and the ECL intensity is decreased for pH values more than 7.5 which can be related to inhibition the oxidation of luminol in alkaline medium [47]. Thus, the detection solution of pH 7.5 was selected for the optimal experiments. Figure 7b shows the concentration of Au@CeO_2/f-CNTs effect on ECL response of the resulting sandwich immunosensor. As observed, the ECL intensity is increased with increasing the concentration of Lu/Au@CeO_2/f-CNTs up to 2 g/L, and the ECL intensity is decreased for Lu/Au@CeO_2/f-CNTs concentration more than 2 g/L which attributed to hindrance of electron transfer excessive concentration [48]. Therefore, 2 g/L was chosen as the optimal concentration of Lu/Au@CeO_2/f-CNTs for the next experiment.

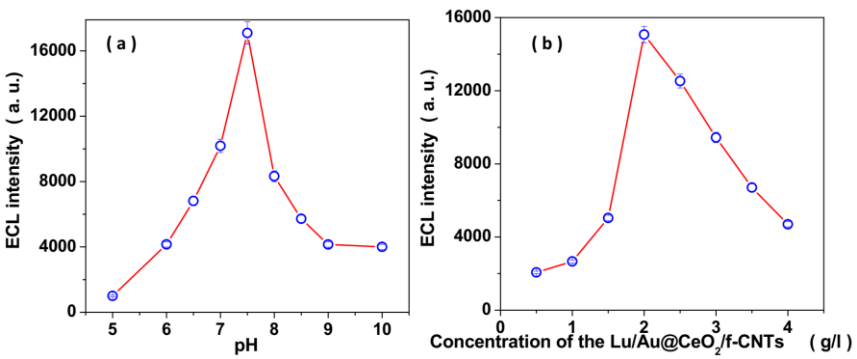

Figure 7. The effects of (a) pH of test solution and (b) concentration of the Lu/Au@CeO_2/f-CNTs on the response of ECL intensity of Ab_2/DA@SiO_2/IAg/BSA/Ab_1/Lu/Au@CeO_2/f-CNTs

Furthermore, Figure 8 shows the pulse potential, pulse time, pulse period and initial potential effects on ECL signal where indicated to the ECL intensity for the resulting sandwich immunosensor and I_0 is the ECL intensity in blank condition. As observed from the Figure 8a, the pulse potential effect in the range from 0.1V to 0.7V on the I/I_0 as response of ECL intensity exhibits that the response of ECL intensity is increased with increasing the of pulse potential up to 0.5 V which correlated with enhancement the luminol oxidation rate [49], and for pulse potential more than 0.5 V, the response of ECL intensity is decreased because of decrease of the stability of the sandwich immunosensor. Accordingly, 0.5 V was chosen as the optimal pulse potential for the optimal experiments. It can be found from Figure 8b that the optimal pulse time is 0.1 s. When the pulse time is longer than 0.1s, the diffusion layer on the surface of the electrode becomes thicker and it is difficult to recover in the next period [50]. Figure 8c displays the pulse period effect on ECL intensity that the pulse period of 10 s shows highest ECL intensity which can be correlated with complete electrochemical reaction of luminal in solution test. Figure 8d shows the initial potential effect on ECL intensity in the range from -0.7 V to -0.2 V. As seen, the maximum ECL intensity is obtained at -0.5 V that it may be related to favorable diffusion controlled reaction at -0.5 V [51]. Therefore, -0.5 V and 10s are selected as the optimum initial potential and pulse period for following measurements, respectively.

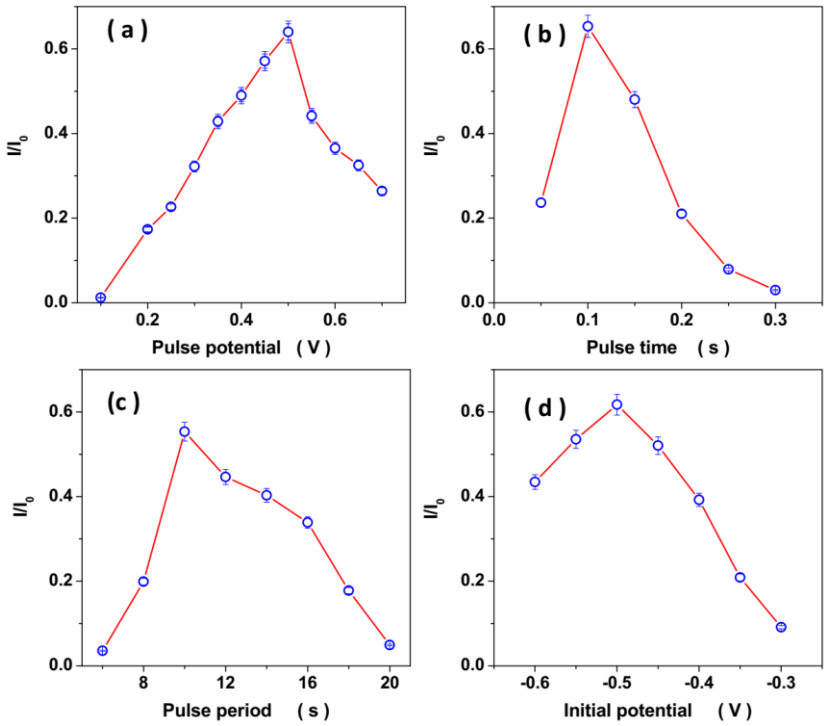

Figure 8. (a) Pulse potential, (b) pulse time, (c) pulse period and (d) initial potential effects on ECL signal.

Figure 9 shows the immunosensor response to different concentrations of insulin under the optimal experimental conditions and obtained calibration plot. As observed, the ECL response is

decreased with increasing insulin concentration. The detection limit and linear range of immunosensor are obtained 17 ng/ml and 10^{-4} ng/ml to 50 ng/ml, respectively. The results of this study are compared with the other previously reported methods in Table 1. It is observed from Table 1 that acceptable linear range and lower detection limit is obtained for Ab_2/DA@SiO_2/IAg/BSA/Ab_1/Lu/Au@CeO_2/f-CNTs due to the good quenching effect of DA@SiO_2 on Lu/Au@CeO_2/f-CNTs, significant specific surface and great conductivity of Au and CeO_2 nanoparticles and f-CNTs, and excellent stability, biocompatibility and catalytic properties of Au nanoparticles.

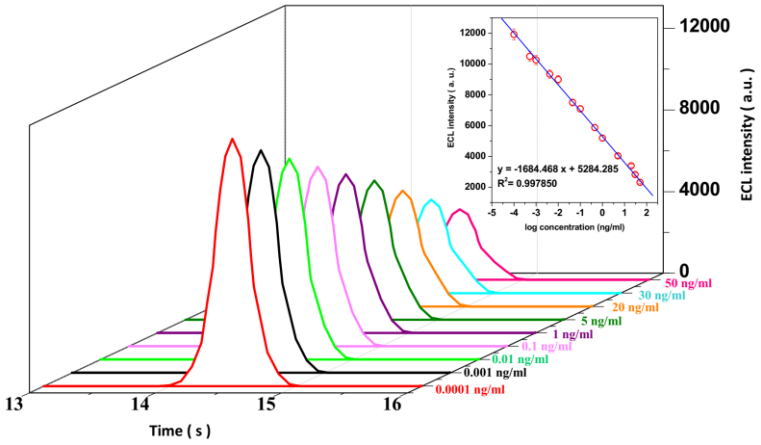

Figure 9. Ab_2/DA@SiO_2/IAg/BSA/Ab_1/Lu/Au@CeO_2/f-CNTs immunosensor response to different concentrations of insulin under the optimal experimental conditions and obtained calibration plot

Table 1. Comparison the obtained sensing results of the Au@CeO2/f-CNTs/GCE with previously reported insulin sensors.

Electrodes	**Technique**	**Linear range (ng/l)**	**Detection limit (ng/l)**	**Ref.**
Au@CeO2/f-CNTs/GCE	ECL	$0.1–5\times10^4$	0.017	This work
Au nanoparticle- doped Pb (II)-β-cyclodextrin	ECL	$0.1–10^4$	0.042	[52]
Carboxyl poly(9,9-dioctyfluorenyl-2,7-diyl) dots	ECL	$0.01–10^5$	0.003	[53]
Arboxyl-functionalized g-C_3N_4	ECL	$0.1–2\times10^4$	0.033	[54]
Fullerene nano-materials/bovine serum albumin@luminol	ECL	$0.1–10^6$	0.040	[55]
Chitosan/$Ru(bpy)_3^{2+}$/silica nanoparticles	ECL	$0.1–10^4$	0.042	[56]
MWCNTs@SnS_2@CdS	Photoelectrochemistry	$0.1–5\times10^3$	0.03	[57]
Polydimethylsiloxane	Microsphere-based immunoassays	$300–10^3$	260	[58]
Chitosan/CNTs/GCE	Amperometry	94100–2823000	28230	[59]

Figure 10 depicts the selectivity and anti-interference capability of the prepared immunosensor for determination of insulin through ECL technique. As seen, the proposed ECL sensor shows the

remarkable response to addition 0.1 ng/ml insulin, and responses to addition 10 ng/ml of glucose (GL), dopamine (DA), carcino-embryonic antigen (CEA), ascorbic acid (AA), B-type natriuretic peptide (BNP), cardiac troponin I (cTnI) and BSA are ignorable. Therefore, the interfering substances do not interfere with the determination of insulin using Ab_2/DA@SiO_2/IAg/BSA/Ab_1/Lu/Au@CeO_2/f-CNTs immunosensor.

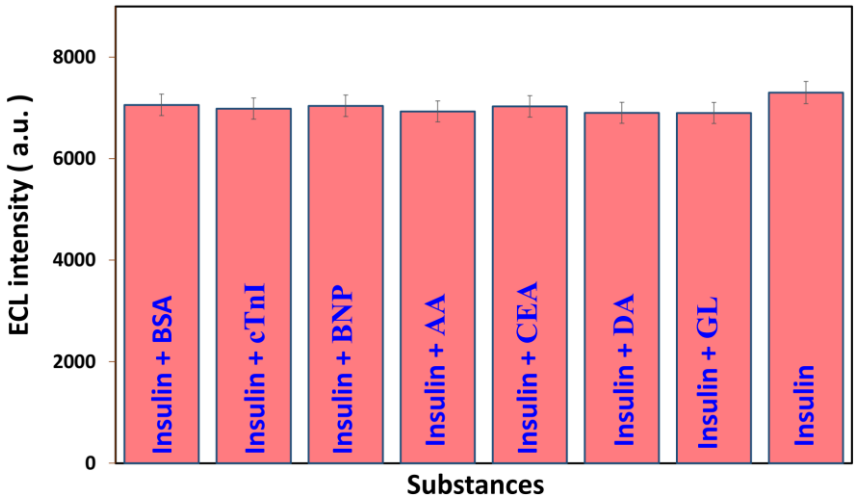

Figure 10. The ECL intensity response of Ab_2/DA@SiO_2/IAg/BSA/Ab_1/Lu/Au@CeO_2/f-CNTs immunosensor to addition 0.1 ng/ml insulin, and responses to addition 10 ng/ml interferents.

3.3 Analysis of real sample

The precision and applicability of the proposed ECL immunosensor to determination of insulin were investigated in blood serum specimens of athletes as real samples. The real human serum samples were provided from five volunteers aged 18 to 21 years 30 minutes after glucose administration. Before the measurements, the blood serum specimens were centrifuged at 1000 rpm for 10 minutes and the obtained supernatants were added to 0.1M CBS pH 7.5 in equal volume ratio. Afterward, the proposed immunosensor was utilized for determination of the concentration of insulin in the prepared real samples under optimum conditions. Table 2 shows the results of average of 5 times determinations of insulin for each specimen through the ECL immunosensor and ELISA techniques, respectively. As seen, the obtained results by ECL immunosensor are very close to the results of ELISA method, illustrating the good agreement and high accuracy between two techniques. Table 3 also shows the results of analytical applicability of ECL immunosensor using standard addition method, demonstrating to achieve the acceptable recovery (100.60 to 94.85%) and RSD (3.11 to 1.84 %) values, and verification of feasibility of the proposed ECL immunosensor for determination serum insulin level in athletes.

Table 2. Results of determination of content of insulin in prepared real serum sample of 5 young volunteers aged 18 to 21 years by ECL immunosensor and ELISA techniques.

Sample	Content of insulin in prepared real serum sample (ng/ml)			
	ECL immunosensor	RSD (%)	ELISA	RSD (%)
S1	1.410	±1.40	1.387	±1.72
S2	1.523	±1.60	1.578	±2.13
S3	1.477	±1.71	1.428	±2.10
S4	1.323	±1.24	1.287	±1.54
S5	1.389	±2.05	1.410	±1.40

Table 3. Results of analytical applicability of ECL immunosensor using standard addition method for determination serum insulin level in athletes.

Added (ng/ml)	Measured (ng/ml)	Recovery (%)	RSD (%)
0.500	0.491	98.20	±1.84
1.000	1.006	100.60	±1.95
1.500	1.493	99.53	±2.24
2.000	1.897	94.85	±3.11

4. CONCULUSION

This study was performed to construct an ECL immunoassay based on sandwich structure of Au@CeO_2/f-CNTs and Ab_2/DA@SiO_2 and application in the measurement of serum insulin level in athletes. For construction the immunosensor based on luminol-O_2 system, Au@CeO_2/f-CNTs and combined with luminol, and DA@SiO_2 used as quencher of ECL signal, and the antibodies were modified the composites surface for enhancement of sensitivity of immunosensor. Results of structural and morphological analyses confirmed successful synthesis of DA@SiO_2 and Au@CeO_2/f-CNTs nanocomposites. The optimal condition were investigated for achievement of maximum ECL signal, and results showed that optimal concentration of Lu/Au@CeO_2/f-CNTs and pH value were 2 g/L and 7.5, respectively, and optimal experimental condition of single-cycle pulse were -0.5 V and 10s as the optimum initial potential and pulse period, respectively. Moreover, 0.5 V and 0.1 s were chosen as the optimal pulse potential and optimal pulse time, respectively. Results showed under the optimal experimental conditions, immunosensor shows high sensitivity and anti-interference capability to determination of insulin, and the detection limit and linear range of immunosensor were obtained 17 ng/ml and 10-4 ng/ml to 50 ng/ml, respectively. The precision and applicability of the proposed ECL immunosensor to determination of insulin were investigated in blood serum specimens of athletes as

real samples, and results indicated to the acceptable recovery and RSD values, and verification of feasibility of the proposed ECL immunosensor for determination serum insulin level in athletes.

References

1. K. Nandi, D.J. Sen and D. Saha, *International Journal of Pharmacy & Life Sciences*, 11 (2020) 7042.
2. H. Ding, X. Bao, Z. Jamili-Shirvan, J. Jin, L. Deng, K. Yao, P. Gong and X. Wang, *Materials & Design*, 210 (2021)
3. F. Shabanpoor, F. Separovic and J.D. Wade, *Vitamins & Hormones*, 80 (2009) 1.
4. Y. Yang, F. Sun, H. Chen, H. Tan, L. Yang, L. Zhang, J. Xie, J. Sun, X. Huang and Y. Huang, *Science of The Total Environment*, 758 (2021) 143631.
5. H. Karimi-Maleh, Y. Orooji, F. Karimi, M. Alizadeh, M. Baghayeri, J. Rouhi, S. Tajik, H. Beitollahi, S. Agarwal and V.K. Gupta, *Biosensors and Bioelectronics*, 184 (2021) 113252.
6. W.S. Borgnakke, *Diabetes research and clinical practice*, 157 (2019) 107839.
7. Q. Jiang, S. Jin, Y. Jiang, M. Liao, R. Feng, L. Zhang, G. Liu and J. Hao, *Molecular neurobiology*, 54 (2017) 594.
8. F.J. DiMenna and A.D. Arad, *BMC Sports Science, Medicine and Rehabilitation*, 10 (2018) 1.
9. Q. Zou, P. Xing, L. Wei and B. Liu, *Rna*, 25 (2019)
10. Y. Xie, X. Meng, D. Mao, Z. Qin, L. Wan and Y. Huang, *ACS Applied Materials & Interfaces*, 13 (2021)
11. Y. Orooji, B. Tanhaei, A. Ayati, S.H. Tabrizi, M. Alizadeh, F.F. Bamoharram, F. Karimi, S. Salmanpour, J. Rouhi and S. Afshar, *Chemosphere*, 281 (2021) 130795.
12. S. Gancheva, T. Jelenik, E. Alvarez-Hernandez and M. Roden, *Physiological reviews*, 98 (2018) 1371.
13. X. Ji, C. Hou, M. Shi, Y. Yan and Y. Liu, *Food Reviews International*, (2020) 1.
14. P.R. Hirschberg, P. Sarkar, S.B. Teegala and V.H. Routh, *Journal of neuroendocrinology*, 32 (2020) e12773.
15. W. Tang, S. Wan, Z. Yang, A.E. Teschendorff and Q. Zou, *Bioinformatics*, 34 (2018) 398.
16. X. Li, Q. Yu, X. Chen and Q. Zhang, *Journal of Magnesium and Alloys*, (2021)
17. Y. Zou, H. Wu, X. Guo, L. Peng, Y. Ding, J. Tang and F. Guo, *Current Bioinformatics*, 16 (2021) 274.
18. B. Sarmento, A. Ribeiro, F. Veiga and D. Ferreira, *Biomedical Chromatography*, 20 (2006) 898.
19. C. Toriumi and K. Imai, *Analytical chemistry*, 74 (2002) 2321.
20. Y. Shen, W. Prinyawiwatkul and Z. Xu, *Analyst*, 144 (2019) 4139.
21. A. Zhang, W. Guo, H. Ke, X. Zhang, H. Zhang, C. Huang, D. Yang, N. Jia and D. Cui, *Biosensors and Bioelectronics*, 101 (2018) 219.
22. L. Chen, Y. Tang, K. Wang, C. Liu and S. Luo, *Electrochemistry communications*, 13 (2011) 133.
23. A. Dolati, M. Ghorbani and M. Ahmadi, *Journal of Electroanalytical Chemistry*, 577 (2005) 1.
24. X. Nie, R. Zhang, Z. Tang, H. Wang, P. Deng and Y. Tang, *Nanomaterials*, 10 (2020) 1356.
25. M. Ibrahim, H. Ibrahim, N.B. Almandil, M.A. Sayed, A.N. Kawde and Y. Aldaqdouq, *Electroanalysis*, 32 (2020)
26. S. Santangelo, *Surface and Interface Analysis*, 48 (2016) 17.
27. B. Xing, W. Zhu, X. Zheng, Y. Zhu, Q. Wei and D. Wu, *Sensors and Actuators B: Chemical*, 265 (2018) 403.
28. X. Sun, Y. Zhu and X. Wang, *Sensors (Basel, Switzerland)*, 11 (2011) 11679.

29. N.K. Sethy, Z. Arif, P.K. Mishra and P. Kumar, *Journal of Polymer Engineering*, 39 (2019) 679.
30. H. Luo, C. Gu, W. Zheng, F. Dai, X. Wang and Z. Zheng, *Rsc Advances*, 5 (2015) 13470.
31. M. Voicescu, M. Vasilescu and A. Meghea, *Journal of Fluorescence*, 10 (2000) 229.
32. Y. Koizumi and Y. Nosaka, *The Journal of Physical Chemistry A*, 117 (2013) 7705.
33. C.V. Raju and S.S. Kumar, *Scientific Reports*, 11 (2021) 6932.
34. T. Ma and H. Wu, *Journal of Chemistry*, 2020 (2020) 1.
35. L. Yang, Y. Jia, D. Wu, Y. Zhang, H. Ju, Y. Du, H. Ma and Q. Wei, *Analytical chemistry*, 91 (2019) 14066.
36. Y. Mikami, A. Dhakshinamoorthy, M. Alvaro and H. Garcia, *Catalysis Science & Technology*, 3 (2013) 58.
37. B. Haghighi and S. Bozorgzadeh, *Analytica chimica acta*, 697 (2011) 90.
38. X. Pang, J. Li, Y. Zhao, D. Wu, Y. Zhang, B. Du, H. Ma and Q. Wei, *ACS Appl Mater Interfaces*, 7 (2015) 19260.
39. H. Chu, W. Guo, J. Di, Y. Wu and Y. Tu, *Electroanalysis: An International Journal Devoted to Fundamental and Practical Aspects of Electroanalysis*, 21 (2009) 1630.
40. A. Ali, B. Xing, M.S. Khan, N. Ma, R. Manzoor, D. Wu and Q. Wei, *Journal of Electroanalytical Chemistry*, 862 (2020) 113970.
41. N. Huang, S. Zhang, L. Yang, M. Liu, H. Li, Y. Zhang and S. Yao, *ACS applied materials & interfaces*, 7 (2015) 17935.
42. T. Zhang, Z. Yang, L. Wang, X. Zhao and Q.-C. Zhuang, *International Journal of Electrochemical Science*, 13 (2018) 8322.
43. C. Cardona, A. Torres, J. Miranda-Vidales, J. Pérez, M. González-Chávez, H. Herrera-Hernández and L. Narváez, *International Journal of Electrochemical Science*, 10 (2015) 1966.
44. F. Yang, J. Han, Y. Zhuo, Z. Yang, Y. Chai and R. Yuan, *Biosensors and Bioelectronics*, 55 (2014) 360.
45. H. Yue, Y. Zhou, P. Wang, X. Wang, Z. Wang, L. Wang and Z. Fu, *Talanta*, 153 (2016) 401.
46. G.-C. Fan, H. Zhu, D. Du, J.-R. Zhang, J.-J. Zhu and Y. Lin, *Analytical chemistry*, 88 (2016) 3392.
47. C. Xiao, D.A. Palmer, D.J. Wesolowski, S.B. Lovitz and D.W. King, *Analytical chemistry*, 74 (2002) 2210.
48. Z. Guo, T. Hao, S. Du, B. Chen, Z. Wang, X. Li and S. Wang, *Biosensors and Bioelectronics*, 44 (2013) 101.
49. E.M. Gross, S.S. Maddipati and S.M. Snyder, *Bioanalysis*, 8 (2016) 2071.
50. Y. Lin, H. Dai, G. Xu, T. Yang, C. Yang, Y. Tong, Y. Yang and G. Chen, *Microchimica Acta*, 180 (2013) 563.
51. F. Li, Y. Yu, H. Cui, D. Yang and Z. Bian, *Analyst*, 138 (2013) 1844.
52. H. Ma, X. Li, T. Yan, Y. Li, H. Liu, Y. Zhang, D. Wu, B. Du and Q. Wei, *ACS applied materials & interfaces*, 8 (2016) 10121.
53. H. Zhang, F. Zuo, X. Tan, S. Xu, R. Yuan and S. Chen, *Biosensors and Bioelectronics*, 104 (2018) 65.
54. H. Ma, Y. Liu, Y. Zhao, L. Li, Y. Zhang, D. Wu and Q. Wei, *Journal of Electroanalytical Chemistry*, 818 (2018) 168.
55. Y. Wang, H. Sha, H. Ke, X. Xiong and N. Jia, *Electrochimica Acta*, 290 (2018) 90.
56. H. Ma, X. Li, T. Yan, Y. Li, H. Liu, Y. Zhang, D. Wu, B. Du and Q. Wei, *ACS Applied Materials & Interfaces*, 8 (2016) 10121.
57. Y. Liu, Y. Zhang, D. Wu, D. Fan, X. Pang, Y. Zhang, H. Ma, X. Sun and Q. Wei, *Biosensors and Bioelectronics*, 86 (2016) 301.
58. N. Cohen, P. Sabhachandani, S. Sarkar, L. Kahanovitz, N. Lautsch, S.J. Russell and T. Konry, *Microchimica Acta*, 184 (2017) 835.

59. M. Zhang, C. Mullens and W. Gorski, *Analytical Chemistry*, 77 (2005) 6396.